Journal of Environmental Management 330 (2023) 117105

Contents lists available at ScienceDirect

Journal of Environmental Management

journal homepage: www.elsevier.com/locate/jenvman

Research article

Transmission paths and source areas of near-surface ozone pollution in the Yangtze River delta region, China from 2015 to 2021

Youru Yao [a], Wei Wang [b], Kang Ma [a], Huarong Tan [a], Yong Zhang [c], Fengman Fang [a], Cheng He [d,*]

[a] Key Laboratory of Earth Surface Processes and Regional Response in the Yangtze-Huaihe River Basin, Anhui Province, School of Geography and Tourism, Anhui Normal University, Wuhu, 241002, China
[b] Nanjing Institute of Environmental Sciences, Ministry of Ecological Environment, Nanjing, 210042, China
[c] Department of Geological Sciences, University of Alabama, Tuscaloosa, AL, 35487, USA
[d] Institute of Epidemiology, Helmholtz Zentrum München – German Research Center for Environmental Health (GmbH), Neuherberg, 85764, Germany

ARTICLE INFO

Keywords:
Ozone
Transmission path
Source contribution
Yangtze river delta region

ABSTRACT

Near-ground ozone in the Yangtze River Delta (YRD) region has become one of the main air pollutants that threaten the health of residents. However, to date, the transport behavior and source areas of ozone in the YRD region have not been systematically analyzed. In this study, by combining the ozone observational record with a HYSPLIT (hybrid single-particle Lagrangian integrated trajectory) model, we tried to reveal the spatiotemporal regularity of the airflow transport trajectory of ozone. Spatially, high ozone concentrations mainly clustered in industrial cities and resource-based cities. Temporally, the center of the ozone pollution shifted westward of Nanjing from 2015 to 2021. With the passage of time, the influence of meteorological elements on the ozone concentration in the YRD region gradually weakened. Marine atmosphere had the most significant impact on the transmission path of ozone in Shanghai, of which the trajectory frequency in 2021 accounted for 64.21% of the total frequency. The transmission trajectory of ozone in summer was different from that in other seasons, and its transmission trajectory was mainly composed of four medium-distance transmission paths: North China-Bohai Sea, East China Sea-West Pacific Ocean, Philippine Sea, and South China Sea-South China. The contribution source areas mainly shifted to the southeast, and the emission of pollutants from the Shandong Peninsula, the Korean Peninsula-Japan, and the Philippine Sea-Taiwan area increased the impact of ozone pollution in the Shanghai area from 2019 to 2021. This study identified the regional transport path of ozone in the YRD region and provided a scientific reference for the joint prevention and control of ozone pollution in this area.

1. Introduction

Ozone is a typical secondary pollutant in the atmosphere, which is produced by the photochemical reaction of primary pollutants (such as volatile organic compounds (VOCs) and nitrogen oxides (NO_x)) under sunlight (Atkinson, 2000; Klemm et al., 2000). Surface ozone has strong oxidizing properties and is one of the main pollutants of photochemical smog (Dommen et al., 1995). It seriously affects the physiological processes of vegetation, grain crops, and human health (Yi et al., 2018; Xu et al., 2020). For example, high concentrations of near-ground ozone (120 μg m^{-3}) can significantly reduce the release of VOCs from flowers (by 25%–30%) over a distance of 4.5 m, making flowers less attractive to pollinators (Farre-Armengol et al., 2016). In addition, tropospheric ozone strongly stimulates the respiratory tract of organisms, thereby increasing residents' risk of developing upper and lower airway inflammation, asthma, allergic rhinitis, and even premature mortalities (Eastham and Barrett, 2016; Krishna et al., 1996). Over the past 30 years, there has been a downward trend in troposphere ozone concentrations in some regions (North America, Europe, etc.) (~3%), due to continuous efforts to control emissions (Schultz et al., 2017). Meanwhile, 100.6 million U.S residents are currently exposed to high levels of surface ozone concentrations (>70 μg m^{-3}) (Zhang et al., 2014). Several studies have reported increasing ozone trends of 1–2 ppbv•a^{-1} at urban and background sites in eastern China (Li et al., 2019; Ma et al., 2016). Therefore, the prevention and control of tropospheric ozone pollution becomes particularly important under the current environmental

* Corresponding author.
E-mail addresses: yaoyouru@ahnu.edu.cn (Y. Yao), 130301622@qq.com (W. Wang), makang0805@163.com (K. Ma), tanhr@ahnu.edu.cn (H. Tan), yzhang264@ua.edu (Y. Zhang), ffm1974@mail.ahnu.edu.cn (F. Fang), hecheng1130@yahoo.com, cheng.he@helmholtz-muenchen.de (C. He).

https://doi.org/10.1016/j.jenvman.2022.117105
Received 19 October 2022; Received in revised form 29 November 2022; Accepted 19 December 2022
Available online 5 January 2023

conditions.

Urban areas are considered hotspots for ozone pollution due to their concentrated transportation and industrial activities (Hu et al., 2021; Pedruzzi et al., 2019; Shu et al., 2020). In addition, against the background of global warming, human activities have led to the long-term emission of high concentrations of air pollutants and VOCs in urban areas (Huy and Oanh, 2020; Narumi et al., 2009). The stratosphere-troposphere exchange in subtropical cities would bring ozone rich stratospheric air into the troposphere, leading to increased urban ozone pollution (Barrett et al., 2019). Therefore, urban areas have become the main source of ozone pollution. The previous study has shown that the death rate caused by ozone pollution in cities in different regions of the world varies by ~10 times, of which 77% of deaths caused by ozone pollution in the world occur in urban areas of South and East Asia (Malashock et al., 2022). Zheng et al. (2010) confirmed that the daily variation in ozone concentration in the Pearl River Delta metropolitan area was larger than that in rural areas. In addition, the ozone pollution in the Pearl River Delta area has regional and super-regional characteristics. Many studies have suggested that it is challenging to describe the dynamic characteristics of ozone pollution in urban areas due to varied local surface characteristics in different regions (e.g., Franco et al., 2019). Therefore, it is of great practical significance to specifically analyze the temporal and spatial dynamic evolution characteristics of ozone in urban areas to identify the migration process of local ozone pollution.

Ozone pollution has significant regional characteristics. The concentration level of regional ozone is related not only to the emission of local pollution sources, meteorological conditions, terrain and other factors, but also to pollutant diffusion and transport between regions, which play a crucial role in the ozone concentration (Yang et al., 2020; Zhao et al., 2018). The transmission and interaction of ozone between regions should not be completely neglected when exploring and revealing the formation process and occurrence mechanism of urban ozone. Therefore, it is crucial to analyze the transmission, source, and influencing factors of ozone migration between regions (Hu et al., 2021). In general, remote sensing observations and numerical models are widely used to carry out quantitative studies of regional atmospheric pollutant transport (Grell et al., 2005). The numerical simulation model is a practical pathway to reveal the dynamic transport processes and diffusion trajectories of ozone (Jeon et al., 2014; Ranmar et al., 2002). However, studies of ozone transport trajectories and source regions based on numerical simulation models have not been systematically carried out at the micro-scales (urban agglomerations). Further studies are still needed to analyze the distribution characteristics and migration behavior of ozone in micro-scale regions by different meteorological and socio-economic factors.

As the economic growth pole of mainland China, the Yangtze River Delta (YRD) region has one of the most developed industries and the highest population density in China. However, dense populations, agglomerated industries, and heavy traffic have stimulated the occurrence and rapid development of local air pollutants (Huang et al., 2017; Zhao et al., 2019). Studies have shown that in the YRD region, the ozone concentration suggested an increasing trend of 1–3 ppbv•a^{-1} during 2013–2017 (Li et al., 2019). Even during the COVID-19 lockdown, a noticeable the daily maximum 8-h average (MDA8) ozone increase of 44% (from 26 to 38 μg m^{-3}) was observed in the YRD region (Zhu et al., 2021). In addition, in eastern China in May and July, the surface ozone responses to climate variability could have an equal or even greater importance than emission changes of gaseous pollutant (Li et al., 2021a; Shu et al., 2020). Thus, it is important to know the main reason for the increase in ozone concentration in the YRD region.

In summary, this study aims to explore the dynamic characteristics, sources, and transport processes of ozone distribution in urban agglomerations at the meso-micro regional scale. To achieve these goals, the rest of this work contains three subsequent steps: (1) analysis of the variation characteristics of ozone concentration in 41 prefecture-level cities in the YRD region on the temporal and spatial scales; (2) clarification of the influence process of different natural and socio-economic factors on the differences in the spatial distribution of ozone; and (3) elucidation of the transport process and main sources of regional ozone, based on numerical simulation models, taking Shanghai as the research subject.

2. Data and methods

2.1. Study areas

The YRD region is located in the lower reaches of the Yangtze River in China, bordering the Yellow Sea and the East China Sea (Fig. S1). Specifically, there are 41 cities across Shanghai, Jiangsu Province, Zhejiang Province, and Anhui Province in the YRD region. The YRD region is mainly in a subtropical monsoon climate, with abundant rainfall and a humid climate. Complex weather and monsoons can have a major impact on the formation and transport of ozone pollution in the region (Ding et al., 2013).

2.2. Data resources

Ozone concentration and meteorological data were collected simultaneously in 41 cities in the YRD region from January 1, 2015 to December 31, 2021. The ozone concentration data were collected from the national real-time city's air quality release platform in the China National Environmental Monitoring Center (http://106.37.208.233:20036/). We adopted the daily maximum 8-h average (MDA 8) ozone concentration from 195 monitoring stations from 41 cities in the YRD region (Fig. S1). The meteorological data used in building the backward trajectory were the 2015–2020 Global Data Assimilation System (GDAS) (ftp://gus.arlhq.noaa.gov./pub/archives/) provided by the National Center for Environmental Prediction (NCEP), with a spatial resolution of 0.5° × 0.5° and a temporal resolution of 6 h. The sources, types, specific descriptions of land use types, meteorological elements, and socioeconomic elements were shown in Table S1 in Supplementary Materials (SI). A quality control process was conducted on the data at individual sites to remove problematic data points before calculating average ozone concentrations and related parameters for ozone dynamics (specific details were shown in Text S1 of the SI).

2.3. Methodology

2.3.1. Standard deviational ellipse (SDE) analysis

The function of SDE quantitatively describes geographic elements with the center, major axis, and minor axis as the basic parameters (Guo et al., 2021). In this study, the spatial distribution and movement characteristics of the ozone distribution in the YRD region were revealed through the variation in the center of gravity, major axis, and minor axis of the SDE. The SDE formula is expressed by (1) - (3).

$$\overline{X}_w = \frac{\sum_{i=1}^{n} w_i x_i}{\sum_{i=1}^{n} w_i}\ ;\ \overline{Y}_w = \frac{\sum_{i=1}^{n} w_i y_i}{\sum_{i=1}^{n} w_i} \tag{1}$$

$$\sigma_x = \frac{\sqrt{\sum_{i=1}^{n} (w_i x_i \cos\theta - w_i \overline{y}_i \sin\theta)}}{\sum_{i=1}^{n} w_i^2} \tag{2}$$

$$\sigma_y = \frac{\sqrt{\sum_{i=1}^{n} (w_i \overline{x}_i \sin\theta - w_i \overline{y}_i \cos\theta)}}{\sum_{i=1}^{n} w_i^2} \tag{3}$$

In these equations, (x_i, y_i) is the spatial region of the research subject;

w_i is the weight; i is the decision-making unit; x and y represent the relative coordinates of each point from the SDE center, respectively; θ is the rotation angle of the distribution pattern (reflects the direction of the main trends in its ozone distribution); and σ_x and σ_y are the standard deviations of the x-axis and y-axis, respectively.

2.3.2. Hybrid single-particle Lagrangian integrated trajectory model (HYSPLIT)

HYSPLIT is a numerical model for atmospheric calculation and analysis of air pollution transport and diffusion trajectories. The model can systematically analyze the transport, diffusion, and deposition of atmospheric pollutants by calculating the input fields of different meteorological elements, physical processes, and pollutant emission sources. It has been widely used in studying the transport trajectory of air pollution in various regions (Du et al., 2020; Guan et al., 2019). The central city of the YRD region, Shanghai (31.14° N, 121.29° E), was selected as the simulated receiving point, and the air flow simulation height was 500 m. The simulation calculated the 72 h backward trajectory of reaching the receiving point at 0:00, 6:00, 12:00, and 18:00 every day from 2015 to 2020. Subsequently, the angular distance method algorithm was adopted to cluster the backward trajectory of ozone. The specific cluster analysis in the backward trajectory model was showed in Text S2 of the SI.

2.3.3. Geographically and temporally weighted regression (GTWR) model

The temporal dimension was introduced into the GTWR model based on spatial heterogeneity, and the time attribute was linked to the spatial attribute of geographically weighted regression. Therefore, the results of GTWR analysis can better reflect the spatio-temporal dynamic changes of geographical elements, making the estimation of regression model more accurate and reasonable. This model extends the standard geographically weighted regression model with temporal variations and can effectively deal with spatiotemporal non-stationarity. The formula of GTWR is expressed by (4) (Huang et al., 2010).

$$Y_i = \beta_0(u_i, v_i, t_i) + \Sigma_k \beta_k(u_i, v_i, t_i) X_{ik} + \varepsilon_i \ , i = 1, 2, \cdots n \quad (4)$$

In Eq. (4), (u, v_i, t_i) is the spatiotemporal coordinate of the i-th sample point. $\beta_0(u_i, v_i, t_i)$ represents the regression constant of the i-th sample point. X_{ik} is the value of the k-th independent variable at the i-th point. ε_i is the residual. $\beta_k(u, v_i, t_i)$ is the k-th regression parameter of the i-th sample point, and its estimation method is as follows ((5)).

$$\widehat{\beta}(\mu_i, v_i, t_i) = \left[X^T \mathrm{W}(u_i, v_i, t_i) \mathrm{X}\right]^{-1} X^T \mathrm{W}(u_i, v_i, t_i) Y \quad (5)$$

In (5), $\widehat{\beta}(u_i, v_i, t_i)$ is the estimate of $\beta_k(u_i, v_i, t_i)$. The superscript T denotes the transpose of a matrix, X and Y are the vectors of predictors and response variables, respectively, and $\mathrm{W}(u_i, v_i, t_i)$ is the space-time weight matrix. The Gaussian distance function is chosen as W, and the calculation formula of the spatiotemporal distance between samples i and j is expressed by (6).

$$d_{ij} = \sqrt{\delta(u_i - u_j)^2 + (v_i - v_j)^2 + \mu(t_i - t_j)^2} \quad (6)$$

Among them, the choice of bandwidth affected the establishment of space-time weights. In this study, the AICc rule (where AICc represents the corrected Akaike information criterion) was used, and the adaptive bandwidth was selected (Huang et al., 2010).

2.3.4. The potential source contribution factor (PSCF) analysis

The PSCF analysis method for ozone in the YRD region was shown in Text S3 of the SI.

3. Results and discussion

3.1. Temporal variation in the ozone concentration in the YRD region

On the interannual scale, the ozone concentration in the YRD region showed a fluctuating downward trend from 2015 to 2021 (Table S2). Among them, the mean ozone concentration (the 90th percentile of MDA8) peaked in 2017, and its concentration (mean ± one standard deviation) was 151–191 μg m^{-3}. From 2017 to 2020, the ozone concentration exhibited a downward trend, among which, from 2019 to 2020, the decline rate (5.59%) of the ozone concentration was higher than that of other years. On the seasonal scale, the ozone concentrations in spring and summer were higher than those in autumn and winter in the YRD (Fig. 1a). Besides, summer had the highest ozone concentration of all seasons from 2015 to 2020 (Fig. 1b). On the monthly scale, the ozone concentration in May and June was the highest of all months, and the ozone concentration in July was the lowest in summer, with a concentration of 69 μg m^{-3} (Fig. 1b). On a daily scale, the variation characteristics of ozone concentration did not show significant regularity (Fig. 1c). However, high concentrations of ozone showed an aggregation phenomenon in a short period of time, by analyzing the figure of continuous ozone daily variation characteristics (Fig. S2). The reason for this phenomenon was mainly due to high temperatures and weather changes (e.g. temperature inversions, quasi-stationary peaks, etc.) over a short period of time (Mao et al., 2020; Mousavinezhad et al., 2021). On the hourly scale, regardless of the season, the surface ozone concentration increased rapidly after noon, peaked at 18:00 (CST (China Standard Time, UTC+0800)), and then gradually decreased (Fig. 1d). The results indicated that under strong illumination, the ozone concentration lagged in the YRD region, and the lag time was ~6 h. Compared with the ambient air quality standards of China (GB3095-2012), the surface ozone concentration on selected days each year exceeded the secondary standard value (160 μg m^{-3}) from 2016 to 2021 (Table S3). However, in the context of the decline in the ozone concentration in the YRD, there were 17 days in 2021 when the ozone concentration exceeded 160 μg m^{-3}. These results showed that the ozone pollution in the YRD might tend to expand over time.

As precursors, nitrogen oxides (NO_x) and volatile organic compounds (VOCs) directly affect local near-ground ozone concentrations (Krupa and Legge, 1995; Sillman, 1995; Xu et al., 2021). In general, since 2017, the near-ground ozone concentration in the YRD region has shown a downward trend, which was due to the concentrations of ozone precursors (NOx and VOCs) emitted in 2017 were at their peak during this time period (Fig. S3). High concentrations of NOx and VOCs directly contribute to elevated urban ozone concentrations (Sun et al., 2022). In addition, the COVID-19 epidemic after 2019 has also directly weakened the total emissions of NO_x and VOCs in China, which improved local air quality (Li et al., 2021b; Qi et al., 2021). On the seasonal scale, due to the intensified stratospheric-tropospheric exchange and stronger photochemical reactions in spring and summer (Sahu et al., 2021), the ozone concentration in the YRD region in spring and summer was higher than that in autumn and winter. On the other hand, high temperature also promoted biogenic volatile organic compounds (BVOCs) emissions (such as isoprene and terpenes) and enhanced ozone chemical production (Gong et al., 2021; Lu et al., 2019). Previous studies showed that the contribution rate of BVOCs emissions to the local ozone concentration (MDA8) was ~15 ppbv in summer over eastern China (e.g., Lu et al., 2019). The highest ozone concentration in the YRD region occurred in May and June, because May and June were the time periods with the largest urban NO_x emissions in the region, compared with other times (An et al., 2015). In addition, this phenomenon was closely related to the climate of this region. Before June, the local area was mainly controlled by cold high pressure, and NO_x and VOCs were not easy to diffuse and migrate. After June, the YRD region was affected by the marine atmosphere, and the effect of precipitation and wind could directly affect the formation of ozone (Tang et al., 2013).

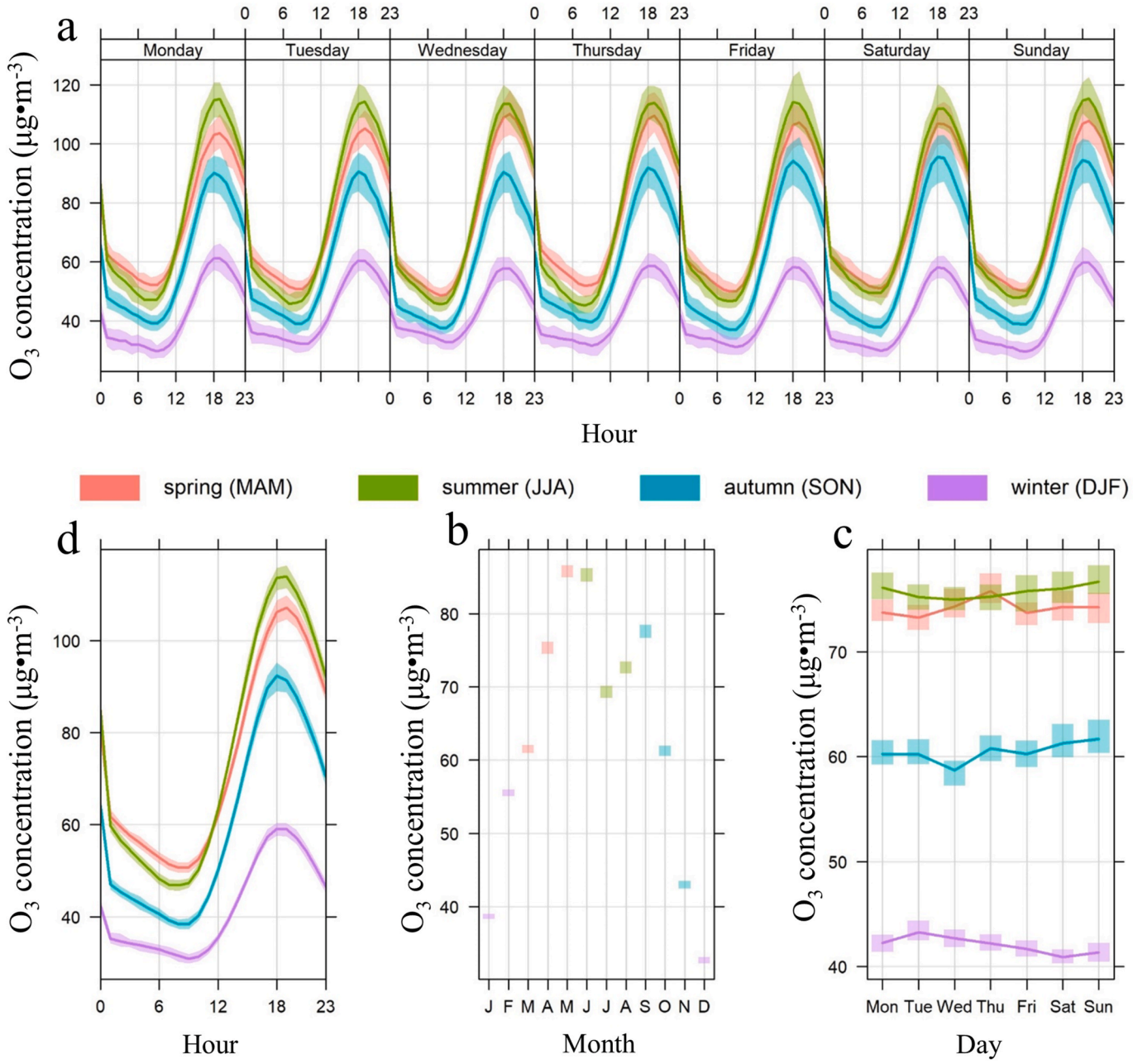

Fig. 1. The average concentration of near-ground ozone at different time scales in the YRD region, 2015–2021 (a), and detailed variation in the ozone concentration at the monthly scale (b), daily scale (c), and hourly scale (d).

The daily and hourly variation characteristics of ozone concentration in the YRD were closely related to local radiation and meteorological conditions, such as typhoons, sea-land breezes, and anticyclones in summer (Xu et al., 2021). Particularly, Xu et al. (2021) found that the sea breeze brought by typhoons leads to a decrease in cloud cover (−25%) and an increase in solar radiation (11%) in the YRD region, resulting in a rapid increase in the ozone concentration in the morning and worsening ozone pollution in the noon and afternoon. On the other hand, the concentration of VOCs released by vegetation also had a significant temporal effect. Intense solar radiation and high temperature aggravated the physiological activities of plants, resulting in the emission of high concentrations of VOCs by vegetation (Gong et al., 2021).

3.2. Spatial variation in the ozone concentration in the YRD region

In general, the spatial distribution of near-ground ozone exhibited planar characteristics in the YRD region (Fig. 2). From 2015 to 2018, the high-concentration ozone area rapidly expanded from the eastern region to the entire YRD region. After that (from 2018 to 2021), there was a shrinking trend in high concentration areas; however, the ozone concentration was still above 120 μg m^{-3} in all areas. Among them, the highest value of ozone concentration appeared in Huzhou City in 2016 (201 μg m^{-3}). There were two main reasons for this phenomenon. On the one hand, Huzhou was surrounded by Hangzhou, Jiaxing, Suzhou, Wuxi and Nanjing. These cities were the major cities that emit by NO_x and VOCs. The high concentration of ozone precursor was the

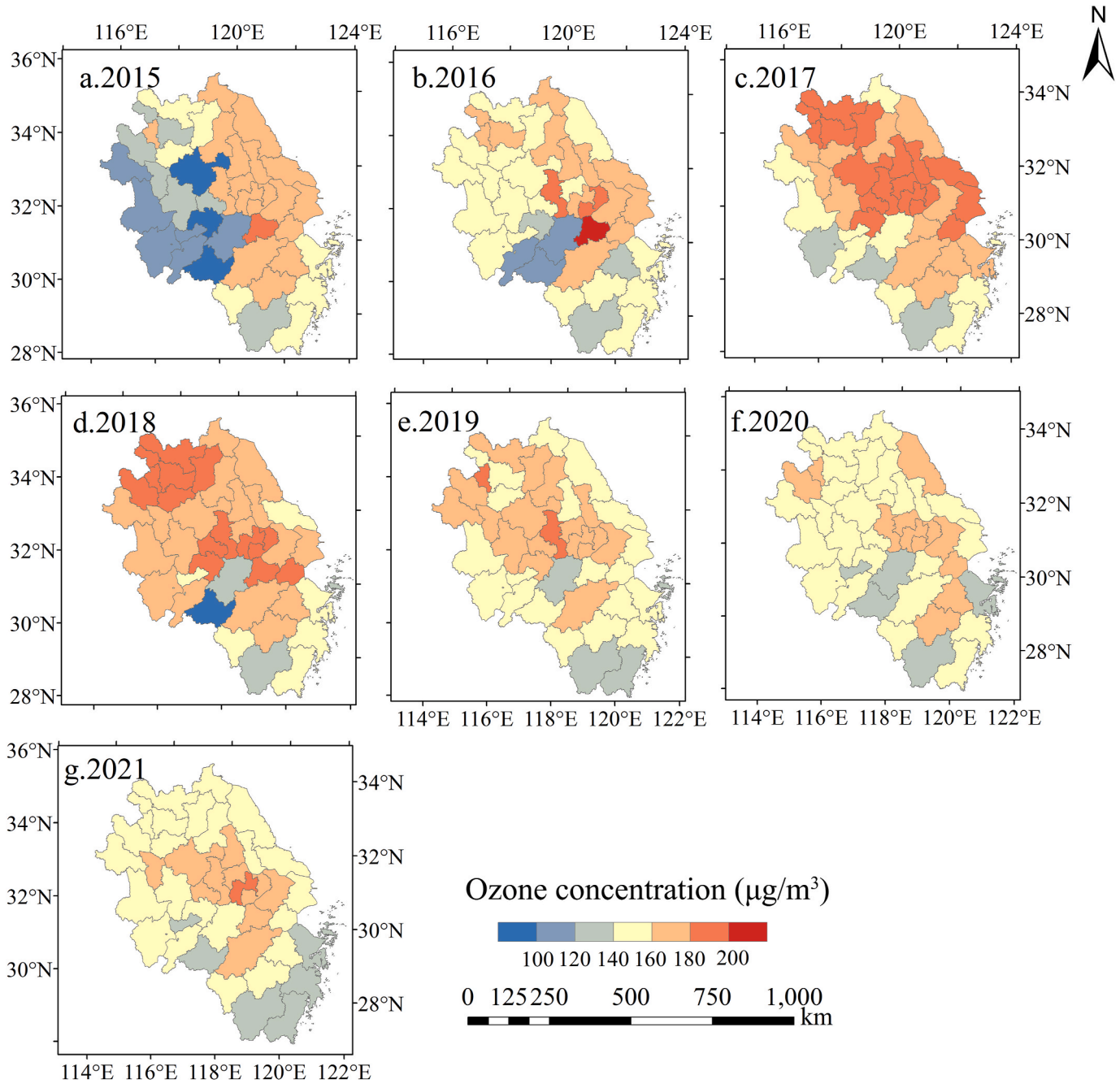

Fig. 2. Evolution of the spatial distribution characteristics of the ozone concentration in the YRD region from 2015 to 2021.

fundamental reason for the increase of local ozone concentration (Wang et al., 2021). On the other hand, Huzhou City was located in the basin terrain, with continuous mountains in the west and southwest. The difficulty in dispersion of air pollutants emitted locally and from neighboring cities has led to a concentration of air pollutants in this region. As a result, ozone in Huzhou City showed high concentration levels. Furthermore, to clearly identify the main cities with ozone pollution, the ozone concentration of all cities in the YRD was extracted from 2015 to 2020 and plotted in Fig. 3. The results showed that the areas with a high ozone concentration were mainly clustered in industrial cities (including Changzhou, Wuxi, Suzhou(a), Nanjing, and Hangzhou) and resource-based cities (including mainly Huaibei (Coal-resource-based city)). In addition, between 2015 and 2021, ozone pollution in these cities was not alleviated.

The spatial distribution of ozone in the YRD region had a significant orientation along southeast-northwest from 2015 to 2021 (Fig. 4). Overall, the ozone pollution in the YRD region was discrete and spanned throughout the region. From 2015 to 2021, the center of the ozone standard deviation ellipse was located in Nanjing, Jiangsu Province, but the center point tended to shift westward. In addition, the area of the ellipse also showed a tendency to expand (from 151683.12 km^2 to 158253.82 km^2 from 2018 to 2021, listed in Table S4). This result also confirmed our above-mentioned finding that the ozone distribution in the YRD region presented the characteristics of planar pollution. From 2015 to 2021, ozone pollution continued to move westward. Although the concentration had a decreasing trend, the pollution area was expanding via dispersion.

The direction of the spatial distribution of ozone in the YRD region

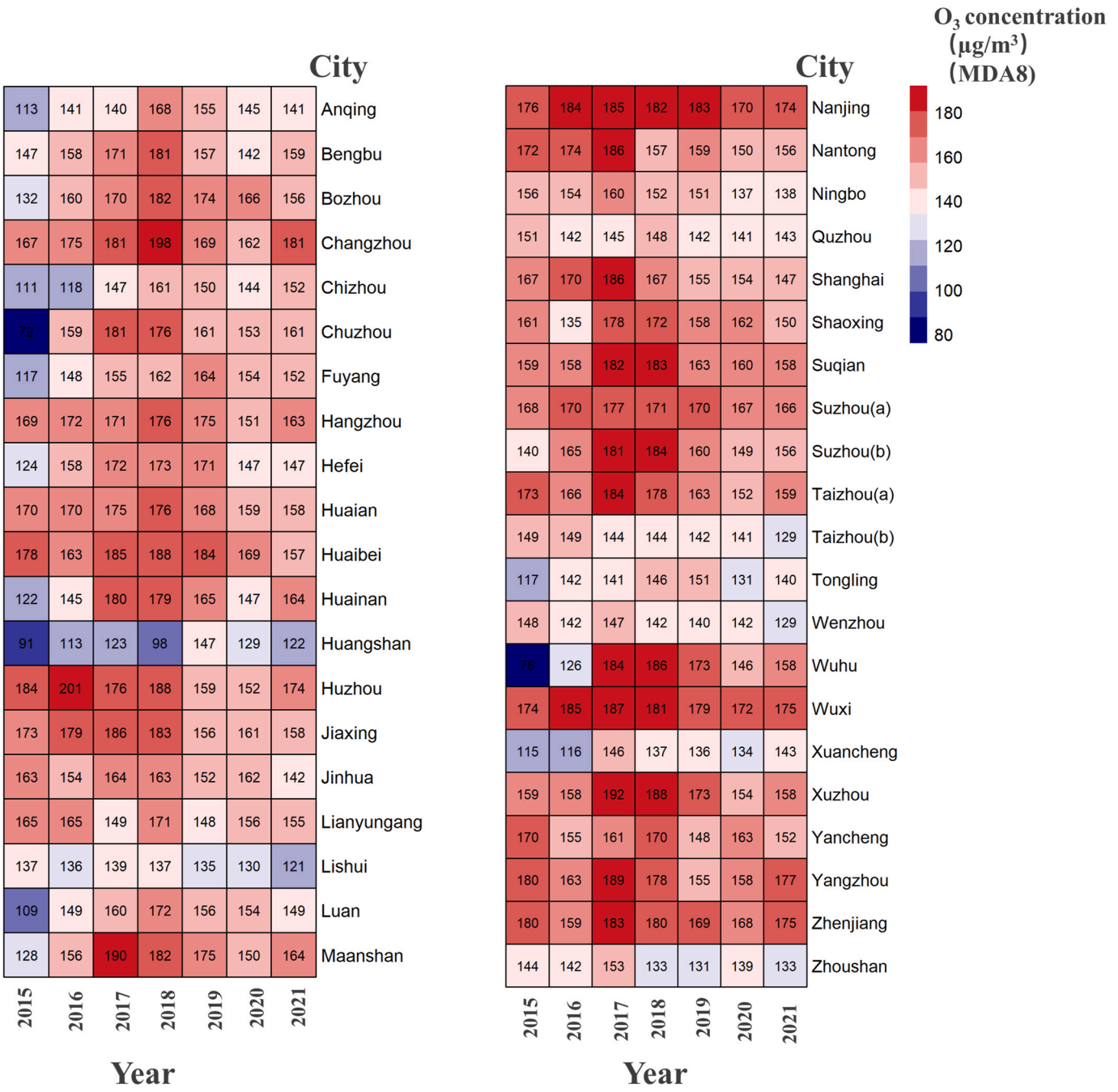

Fig. 3. Variation characteristics of the annual average ozone concentration in different cities in the YRD region in 2015–2020.

was similar to the local prevailing wind direction (southeast wind in the summer and northwest wind in the winter). Moreover, cities with high ozone concentrations were mainly concentrated in the downwind direction, including populated and industrialized cities. Prevailing winds and land-sea breezes have important effects on ozone transport in coastal areas (Stauffer et al., 2015; Wang et al., 2001). High concentrations of ozone and its precursors were exported continuously from their emission sources to receptor regions far downwind on regional, intercontinental, and even hemispheric scales (Monks et al., 2009; Xu et al., 2021). As mentioned above, the concentration of ozone was directly related to NO_x from fossil fuel combustion and VOCs emitted from anthropogenic and biogenic sources (Xu et al., 2021). The eastern part of the YRD region (including three provinces: Shanghai, Jiangsu, and Zhejiang) has remained one of the most densely populated and most industrially developed urban areas in mainland China (Zhang et al., 2017). Therefore, the ozone concentration in this region has always been high. With the development of industrialization and urbanization in the western part of the YRD regions (Anhui Province), the ozone concentration in Anhui Province also showed an upward trend (Sulaymon et al., 2021). Compared with the NO_2 concentration distribution from 2005 to 2010, the NO_2 concentration in Anhui from 2011 to 2016 increased by 13.9%–19.9% (Xie et al., 2018). Based on the above-mentioned analysis, the efficient prevention and control of urban ozone pollution in the YRD region should not only focus on key cities located mainly on the east of the region (such as Shanghai, Nanjing, Hangzhou, etc.), but also prevent ozone pollution from spreading to the west of the region.

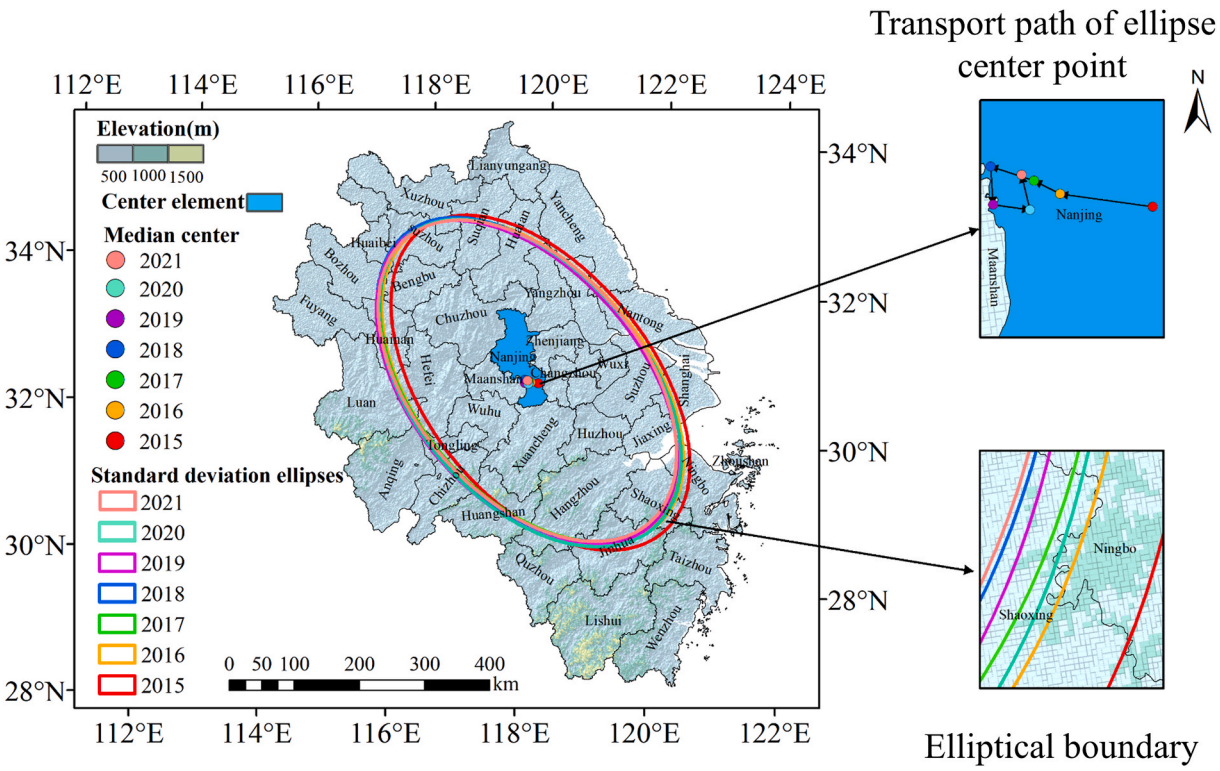

Fig. 4. Time series of the mean center and standard deviational ellipse of the ozone ground-level concentration in the YRD region in 2015–2021 by standard deviational ellipse model.

3.3. Different driving factors affecting the ozone concentration in the YRD region

Twelve potential drivers were selected (including meteorological and socio-economic factors) as explanatory variables of the principal component analysis model, and they were used to explain main causes affecting ozone concentrations in the YRD region. (Tables S5 and S6). Four main factors were screened out, where the largest contribution to ozone concentration in the YRD area was made by industrial elements (e.g. GDP per capita, urbanization rate, NO_x emissions and number of industrial enterprises) (32.23%) (Table S6). In additions, the meteorological elements of rainfall, temperature, relative humidity and sunshine duration had a significant contribution to ozone concentration (22.48%). Local wind speed (11.79%) and SO_x emissions (6.31%) also had an impact on local ozone.

Furthermore, these twelve potential driving factors also were selected as the explanatory variables of the GTWR model, and they were used to explain the reasons affecting the spatial distribution of ozone (Text S4, Table S7, and Fig. 5). Specifically, industrial NO_x emissions (with the regression coefficient of 2.07), urbanization rate (1.04), sunshine hours (0.50), temperature (0.27), and wind speed (0.25) had stimulatory effects on the increase in the ozone concentration in most of the YRD region. Relatively, relative humidity (−0.35) was negatively correlated with the spatial concentration of ozone. The formation of urban tropospheric ozone was a secondary pollutant formed by a series of photochemical reactions of NO_x and VOCs in the presence of solar radiation (Fishman and Crutzen, 1978). The specific chemical process of ozone formation is as follow (Sun et al., 2022):

$$RH + OH \rightarrow R + H_2O \quad \text{(R1)}$$

$$R + O_2(+M) \rightarrow RO_2(+M) \quad \text{(R2)}$$

$$RO_2 + NO \rightarrow RO + NO_2 \quad \text{(R3)}$$

$$RO + O_2 \rightarrow R'CHO(R'COR'') + H_2O \quad \text{(R4)}$$

$$H_2O + NO \rightarrow OH + NO_2 \quad \text{(R5)}$$

$$NO_2 + \langle v + O_2 \rightarrow O_3 + NO \quad \text{(R6)}$$

As seen in *R6*, NO_x emissions and light intensity were direct factors in ozone formation. Therefore, NO_x concentration and sunshine hours were positively correlated with ozone concentration. The inverse correlation between relative humidity and ozone concentration was explained in three main ways. Firstly, a moist, cool environment, weak solar radiation and wet deposition by water vapor reduced ozone concentrations in YRD region. Studies have shown that marine atmosphere aided water vapor transportation to the YRD region. Combined with significant upward air flow, more clouds formed at the medium and low levels, and precipitation was enhanced in the YRD region (Yin et al., 2019). The above results led to a reduction in ozone concentrations in the YRD region (Yin et al., 2019). Secondly, the active species (HO_2• (peroxyhydroxy radicals), HO• (hydroxyl radicals), etc.) in the atmosphere quickly decomposed the ozone into oxygen molecules, reducing the ozone concentration. Finally, the higher the relative humidity is, the stronger the wet scavenging of ozone generation precursors (Gaur et al., 2014).

It was different in the effects of various driving factors on the ozone concentration among regions (2015–2021) (Fig. 5). For example, for Anhui Province, local temperature, sunshine hours, and NO_x concentration showed significant positive effects on ozone accumulation. The contributions of wind speed, SO_2 concentration, and industrial activity to the ozone concentration in Zhejiang Province were greater than those of the other driving factors. The ozone aggregation characteristics in Jiangsu Province were mainly driven by temperature and industrial activity. The driving factors of ozone in Shanghai were different from those in the other three provinces. The clustering of ozone in Shanghai was mainly driven by the level of urbanization and industrial soot

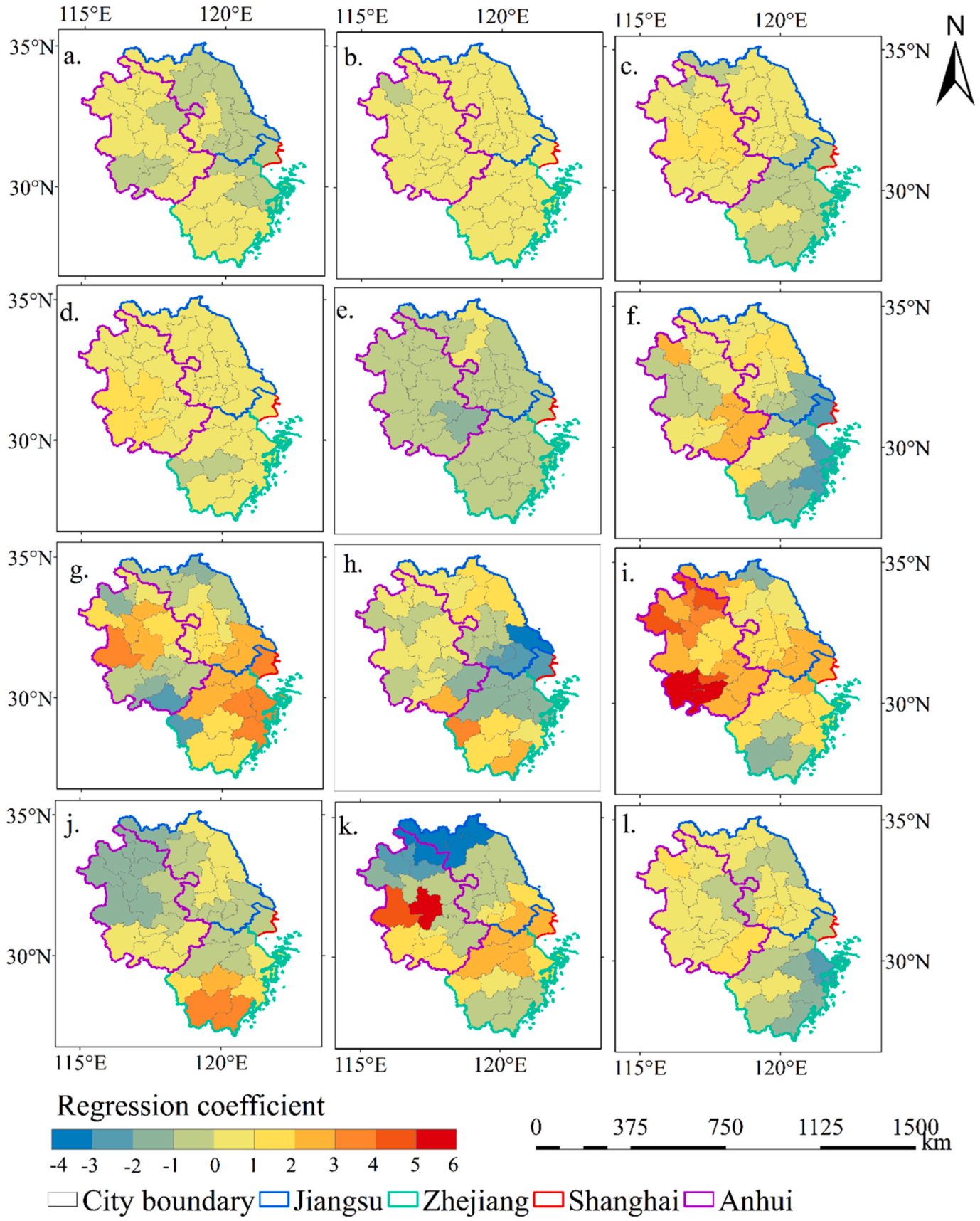

Fig. 5. Influence characteristics of different factors on the spatial distribution of ozone in the YRD region. a: wind speed; b: precipitation; c: temperature; d: sunshine hours; e: relative humidity; f: GDP per capita; g: urbanization rate; h: industrial SO_x emissions; i: industrial NO_x emissions; j: Number of industrial enterprises above designated size; k: industrial soot (dust) emissions; and l: General solid waste utilization rate. The value plotted in this map is regression coefficient of GTWR.

emissions. Compared with other provinces, Anhui Province had a less level of industry and lower emissions of air pollutants. The production of ozone in the atmosphere mainly came from the emission of NO_x in the province and the photochemistry of the atmosphere. Additionally, elevated temperatures and greater solar radiation were related to higher ozone concentrations in Anhui Province (Fig. S4). For Zhejiang Province, the distribution of ozone was related to the emission of its own pollutants. Driven by meteorological elements, transport of ozone in the YRD region also affected the variations in the ozone concentration (Wang and Liao, 2020). Jiangsu and Shanghai are the central and core industrial areas in the YRD region. The distribution characteristics of local ozone pollution were driven by the local urbanization level, air pollutant emissions, and meteorological factors. However, the contribution rate of the outer regions to the ozone concentration in Shanghai and Jiangsu is unclear and requires further study due to the dynamic transport of ozone.

There were spatial differences in the influence of various driving factors on the concentration distribution of ozone in different periods (2015–2020) (Fig. S5). With the passage of time, the influence of meteorological elements on the ozone concentration in the YRD region gradually weakened (Figs. S5a–e). In particular, temperature and precipitation dropped from 0.54 (Regression coefficients of GTWR) and 0.36 to 0.06 and 0.07, respectively. In general, the impact of socioeconomic factors on ozone distribution is more stable than that of meteorological factors (Fig. S5f-l). However, the driving effect of industrial SO_x, NO_x, and soot emissions on ozone distribution showed an increasing trend (Fig. S5h, i & k).

Relative to other years, the ozone concentration in the YRD region showed the highest concentration levels in 2017; therefore, the effects of different factors on the ozone concentration in 2017 were separated out separately (Fig. S6). Compared to Fig. 5, in the western and northern parts of the YRD region, GDP per capita and industrial NO_x emissions contributed more to ozone concentration than other elements in 2017. Besides, For the southeastern part of the YRD region, the urbanization rate had a greater effect on the variation of ozone concentration than other elements. The results have shown that urbanization and industrialization can directly affect the level of ozone concentration in the YRD region. However, the contribution of meteorological elements to ozone remained stable both in other years and in 2017. Therefore, the control of industrial air pollution emissions is the focus of ozone pollution prevention and control in the YRD region.

3.4. Clusters of ozone backward trajectories in Shanghai

The HYSPLIT model was adopted to calculate the backward trajectory of ozone in Shanghai from 2015 to 2021 (Fig. 6). Overall, four main types of transmission trajectories were clustered. The four transmission paths were the Mongolia-North China long-distance trajectory, Japan Sea-East China Sea and Bohai Sea oceanic medium-distance trajectory, and South China-Central China short-distance trajectory. The formation of these trajectories was mainly due to the influence of inland, oceanic, and local transport air masses. The dominance of the three air masses constantly changed at different times. For example, the transport pathway of ozone in Shanghai was dominated by marine atmosphere in 2016, 2017, 2019, and 2021; however, locally transported air masses were the main contributors in 2018 and 2020. It is worth noting that among the three types of air masses, marine atmosphere had the greatest impact on the transmission path of ozone in Shanghai, of which the trajectory frequency in 2021 accounted for 64.21%. High levels of ozone pollution came not only from local emission sources but also from regional and even super-regional characteristics (Zheng et al., 2010). Zheng et al. (2010) found that there were three main ozone transmission trajectories in the Pearl River Delta, namely, 29% of the air mass trajectories passed through mainland China, 35% came from the South China Sea, and 36% passed through the coastlines of the YRD region, Fujian, and Hong Kong. Compared with the ozone transport path in the Pearl River Delta, the ozone transport in the YRD region was more affected by ozone pollution in the interior of mainland China and the Bohai Sea region.

The tropospheric ozone transport path in Nanjing (central point of ozone in the YRD region) has also been further studied (Fig. S7). The results showed that the transport path of ozone in Nanjing was similar to that of ozone in Shanghai from 2015 to 2021. The main source of ozone transport behavior in Nanjing was the marine atmosphere (35%~60%), followed by continental air masses and local air masses. Among them, the marine atmosphere mainly derived from the East China Sea and Bohai Sea area. In addition, consistent with the characteristics of ozone trajectories in Shanghai, local air masses were the most important contributors to ozone in Nanjing in 2017 and 2018.

Furthermore, the backward trajectories of ozone airflow for all days were calculated during different seasons in Shanghai from 2015 to 2021 (Fig. S8). The results indicated that the main transport trajectory of ozone in Shanghai had significant seasonal variations. There were four main transmission routes in spring, autumn and winter, namely the Mongolia-Siberia long-distance trajectory, the Northeast-North China mid-distance trajectory, the Bohai-Japan mid-distance trajectory, and the Central China-South China short-distance trajectory. Among them, except in summer, the highest frequency of ozone transmission trajectories in Shanghai came from the Northeast-North China region (18.97% ~57.78%). However, the transmission trajectory of ozone in summer was different from that in other seasons, and its transmission trajectory was mainly composed of four medium-distance transmission paths: North China-Bohai Sea, East China Sea-West Pacific Ocean, Philippine Sea, and South China Sea-South China. Here, an interesting phenomenon was found: in the summer of low-level ozone concentration years (2019–2021), one or two of the four transmission paths dominated, with a track frequency of more than 35% (even reaching as much as 61.26%). In contrast, in the years with high ozone concentrations (2015–2018), the frequencies of the four transmission trajectories were basically similar, all approximately 20%. In cities in coastal regions, the local tropospheric ozone pollution was becoming worse when the continental air mass and the marine atmosphere were controlled alternately. Air pollutants from continental sources were further involved in intensive photochemical reactions due to continental air masses bringing in large amounts of primary pollutants (NO_x and VOCs) needed for ozone formation, leading to higher ozone levels in marine atmosphere than in coastal cities (Wang et al., 2018a). In addition, when marine atmosphere controlled offshore cities, on the one hand, the titration of NO to ozone was weaker due to the lower concentration of NO in marine atmosphere; on the other hand, the oxidation capacity of marine atmosphere was stronger than that of the near-surface atmosphere, resulting in a faster rate of oxidation of VOCs by hydroxyl radicals, thus facilitating photochemical reactions to generate ozone in the urban troposphere (Wang et al. 2018b, 2019).

3.5. Potential source areas for ozone in Shanghai

Furthermore, potential sources of tropospheric ozone in the Shanghai area were analyzed (Fig. 7). Tropospheric ozone in Shanghai was mainly derived from four regions, namely North China-Northeast China, the Korean Peninsula-Sea of Japan, East and Central China, and Taiwan-East China Sea. From 2016 to 2018, the main contributors to ozone pollution were North China and East China, and their cumulative contribution rate exceeded 50%. However, from 2019 to 2021, the contribution source areas mainly shifted to the east and south, and the emission of pollutants from the Shandong Peninsula, the Korean Peninsula-Japan, and the Philippine Sea-Taiwan area increased the impact of ozone pollution in the Shanghai area. The above-mentioned areas had become the main sources of ozone in Shanghai for two main reasons. On the one hand, the abovementioned regions were urban agglomeration areas, and their own tropospheric ozone pollution status was not optimistic. For example, in the summer of 2015, the maximum

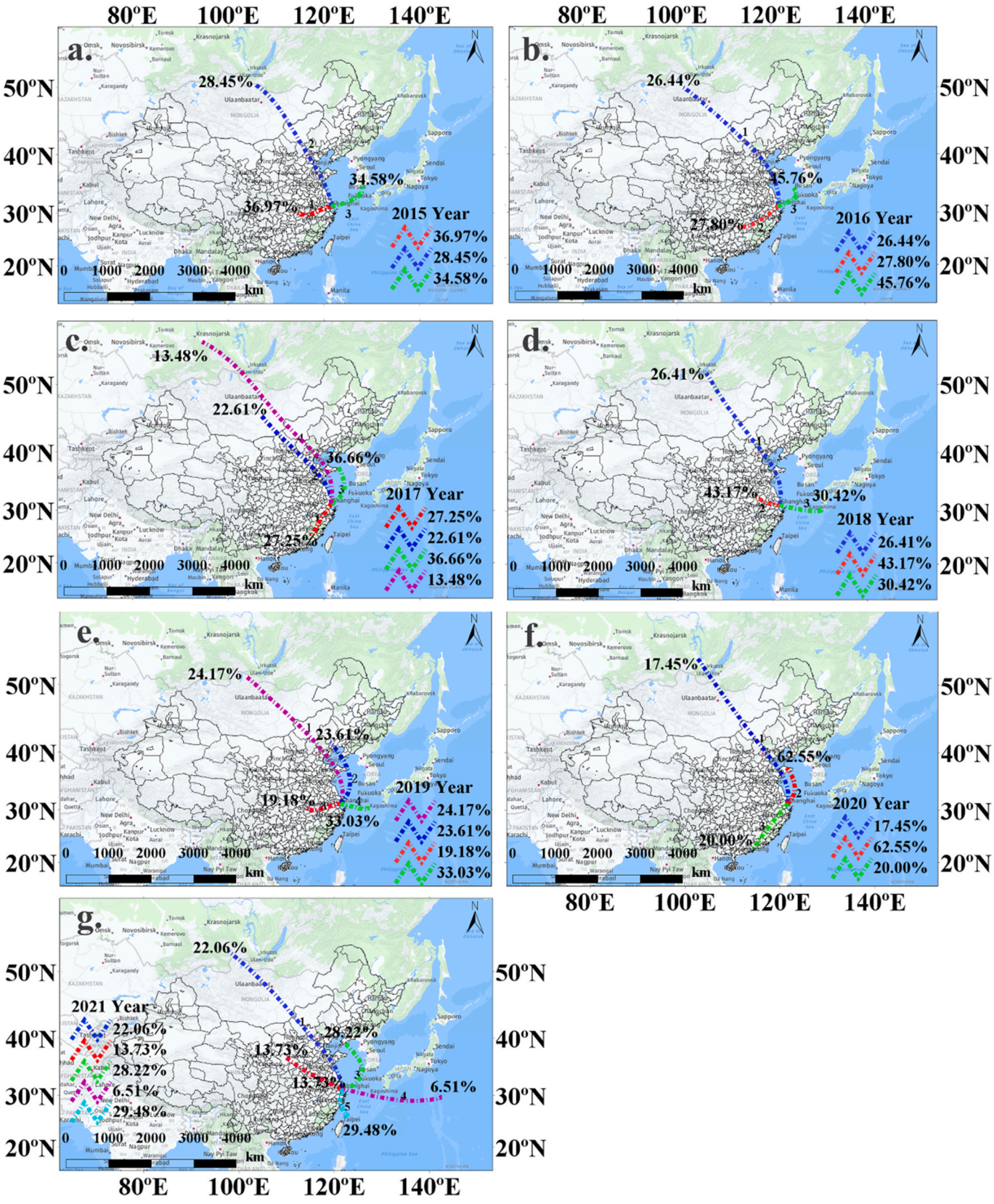

Fig. 6. Clusters of backward trajectories of ozone in Shanghai in 2015–2021. A. 2015; b. 2016; c. 2017; d. 2018; e. 2019; f. 2020; and g. 2021.

MDA8 ozone concentration in North China was 223 μg m^{-3} over the most dramatic areas, and the minimum was 87 μg m^{-3} (Liu et al., 2021). In addition, during 1980–2005, the annual mean surface ozone over Japan showed a clear increasing trend with a linear increase of approximately 2.70 ppbv per decade (Nagashima et al., 2017). The ozone concentrations in South Korea for both E– and L-sites generally increased at a rate of 0.68 ppbv/$year^{-1}$ from 2005 to 2014 (Jung et al., 2018). On the other hand, they were all in the upper wind direction of

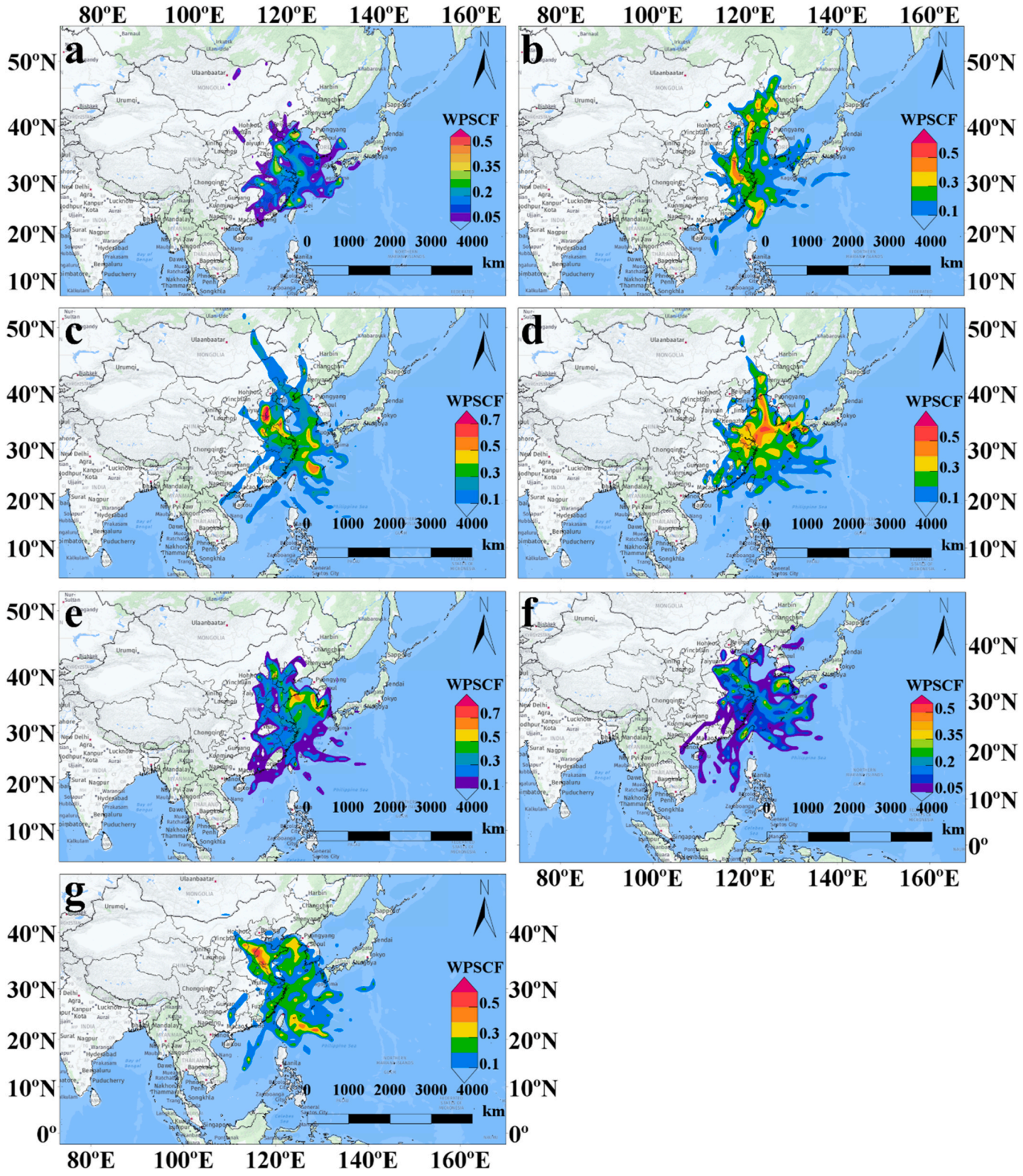

Fig. 7. The potential source contribution for ozone in Shanghai. a. 2015; b. 2016; c. 2017; d. 2018; e. 2019; f. 2020; and g. 2021.

the prevailing wind direction in Shanghai. For example, the winter monsoon (northeasterly wind) and the geostrophic deflection force induced the transport of ozone from North China and the Korean Peninsula to East China. In contrast, the summer monsoon (southwesterly wind) accelerated ozone migration from Taiwan and the Philippine Sea to Shanghai.

4. Conclusion

In this study, Long-term (6 years) ozone data from 41 cities in the Yangtze River Delta (YRD) region were collected to analyze the spatio-temporal dynamics and transport behavior of ozone concentrations in the region. In general, on a long time and spatial scale, ozone

concentrations in the region showed a decreasing trend and the center of ozone emissions was gradually moving westward. Specifically, temporally, the mean ozone concentration (the 90th percentile of MDA8) peaked in 2017 (151–191 μg m^{-3}) during 2015–2020. From 2017 to 2020, the ozone concentration suggested a downward tendency. During this period, 2019 featured the highest decline rate (5.59%) of the ozone concentration. On the hourly scale, regardless of the season, the surface ozone concentration increased rapidly in the afternoon and peaked at 18:00. Spatially, high ozone concentration areas were mainly clustered in industrial cities (inclidng Changzhou, Wuxi, Suzhou, Nanjing, and Hangzhou) and resource-based cities (e.g., Huaibei). From 2015 to 2021, the center of the ozone standard deviation ellipse was shifted westward from Nanjing. In addition, the area of the ellipse also showed a tendency to expand (from 151683.12 km^2 to 158253.82 km^2) from 2018 to 2021. Industrial NO_x emissions, urbanization rate, sunshine hours, temperature, and wind speed had stimulatory effects on the increase in ozone concentration in most of the YRD region. Relatively, relative humidity was negatively correlated with the ozone concentration. In addition, the influence of meteorological conditions gradually weakened during the process, the driving effect of industrial SO_x, NO_x, and soot emissions on ozone distribution showed an increasing trend. Marine atmosphere had a great impact on the transmission path of ozone and the trajectory frequency in 2021 accounted for 64.21% of the whole. The transmission trajectory was mainly composed of four medium-distance transmission paths: North China-Bohai Sea, East China Sea-West Pacific Ocean, Philippine Sea, and South China Sea-South China. The contribution source areas mainly shifted to the east and south. The emission of pollutants from the Shandong Peninsula, the Korean Peninsula-Japan, and the Philippine Sea-Taiwan area increased the impact of ozone pollution in the Shanghai area from 2019 to 2021.

Author contribution

Youru Yao: Methodology, Investigation, Data curation, Writing – original draft. Wei Wang: Investigation, Data curation, Writing – original draft. Kang Ma: Visualization, Investigation, Data curation, Writing – review & editing. Huarong Tan: Investigation, Data curation, Writing – review & editing. Yong Zhang: Writing – review & editing. Fengman Fang; Writing – review & editing. Cheng He: Formal analysis, Supervision, Writing – review & editing.

Declaration of competing interest

The authors declare that they have no known competing financial interests or personal relationships that could have appeared to influence the work reported in this paper.

Data availability

Data will be made available on request.

Acknowledge

This work was supported by Natural Science Research Project of Anhui Educational Committee(KJ 2021A0121), Ph. D research start-up fund (762140), and talent cultivation project (2021xjxm032) of Anhui Normal University.

Appendix A. Supplementary data

Supplementary data to this article can be found online at https://doi.org/10.1016/j.jenvman.2022.117105.

References

An, J.L., Zou, J.N., Wang, J.X., Lin, X., Zhu, B., 2015. Differences in ozone photochemical characteristics between the megacity Nanjing and its suburban surroundings, Yangtze River Delta, China. Environ. Sci. Pollut. Control Ser. 22 (24), 19607–19617.
Atkinson, R., 2000. Atmospheric chemistry of VOCs and NOx. Atmos. Environ. 34 (12–14), 2063–2101.
Barrett, B.S., Raga, G.B., Retama, A., Leonard, C., 2019. A multiscale analysis of the tropospheric and stratospheric mechanisms leading to the march 2016 extreme surface ozone event in Mexico city. J. Geophys. Res. Atmos. 124 (8), 4782–4799.
Ding, A.J., Fu, C.B., Yang, X.Q., Sun, J.N., Zheng, L.F., Xie, Y.N., Herrmann, E., Nie, W., Petaja, T., Kerminen, V.M., Kulmala, M., 2013. Ozone and fine particle in the western Yangtze River Delta: an overview of 1 yr data at the SORPES station. Atmos. Chem. Phys. 13 (11), 5813–5830.
Dommen, J., Neftel, A., Sigg, A., Jacob, D.J., 1995. Ozone and hydrogen peroxide during summer smog episodes over the Swiss Plateau: measurements and model simulations. J. Geophys. Res. Atmos. 100 (D5), 8953–8966.
Du, X.M., Jin, X.M., Zucker, N., Kennedy, R., Urpelainen, J., 2020. Transboundary air pollution from coal-fired power generation. J. Environ. Manag. 270, 110862.
Eastham, S.D., Barrett, S.R.H., 2016. Aviation-attributable ozone as a driver for changes in mortality related to air quality and skin cancer. Atmos. Environ. 144, 17–23.
Farre-Armengol, G., Penuelas, J., Li, T., Yli-Pirila, P., Filella, I., Llusia, J., Blande, J.D., 2016. Ozone degrades floral scent and reduces pollinator attraction to flowers. New Phytol. 209 (1), 152–160.
Fishman, J., Crutzen, P.J., 1978. The origin of ozone in the troposphere. Nature 274 (5674), 855–858.
Franco, D.M.P., Andrade, M.D., Ynoue, R.Y., Ching, J., 2019. Effect of Local Climate Zone (LCZ) classification on ozone chemical transport model simulations in Sao Paulo, Brazil. Urban Clim. 27, 293–313.
Gaur, A., Tripathi, S.N., Kanawade, V.P., Tare, V., Shukla, S.P., 2014. Four-year measurements of trace gases (SO_2, NO_x, CO, and O_3) at an urban location, Kanpur, in Northern India. J. Atmos. Chem. 71 (4), 283–301.
Grell, G., Peckham, S., Schmitz, R., McKeen, S., Frost, G., Skamarock, W., Eder, B., 2005. Fully coupled "online" chemistry within the WRF model. Atmos. Environ. 39 (37), 6957–6975.
Gong, C., Liao, H., Yue, X., Ma, Y.M., Lei, Y.D., 2021. Impacts of ozone-vegetation interactions on ozone pollution episodes in North China and the Yangtze River Delta. Geophys. Res. Lett. 48 (12), e2021GL093814.
Guan, Q.Y., Liu, Z.Y., Yang, L.G., Luo, H.P., Yang, Y.Y., Zhao, R., Wang, F.F., 2019. Variation in PM2.5 source over megacities on the ancient Silk Road, northwestern China. J. Clean. Prod. 208, 897–903.
Guo, B., Wang, X., Pei, L., Su, Y., Zhang, D., Wang, Y., 2021. Identifying the spatiotemporal dynamic of PM2.5 concentrations at multiple scales using geographically and temporally weighted regression model across China during 2015-2018. Sci. Total Environ. 751, 141765.
Hu, M.M., Wang, Y.F., Wang, S., Jiao, M.Y., Huang, G.H., Xia, B.C., 2021. Spatial-temporal heterogeneity of air pollution and its relationship with meteorological factors in the Pearl River Delta, China. Atmos. Environ. 254 (13), 118415.
Huang, B., Wu, B., Barry, M., 2010. Geographically and temporally weighted regression for modeling spatio-temporal variation in house prices. Int. J. Geogr. Inf. Sci. 24 (3), 383–401.
Huang, L., Zhang, C., Bi, J., 2017. Development of land use regression models for PM2.5, SO_2, NO_2 and O_3 in Nanjing, China. Environ. Res. 158, 542–552.
Huy, L.N., Oanh, N.T.K., 2020. Emission control for volatile organic compounds from gasoline stations and implication on ozone-forming potential. Atmos. Pollut. Res. 11 (6), 87–98.
Jeon, W.B., Lee, S.H., Lee, H., Park, C., Kim, D.H., Park, S.Y., 2014. A study on high ozone formation mechanism associated with change of NOx/VOCs ratio at a rural area in the Korean Peninsula. Atmos. Environ. 89, 10–21.
Jung, H.C., Moon, B.K., Wie, J., 2018. Seasonal changes in surface ozone over South Korea. Heliyon 4 (1), e00515.
Klemm, O., Stockwell, W.R., Schlager, H., Krautstrunk, M., 2000. NO_x or VOC limitation in East German ozone plumes? J. Atmos. Chem. 35 (1), 1–18.
Krishna, M.T., Springall, D.R., Frew, A.J., Polak, J.M., Holgate, S.T., 1996. Mediators of inflammation in response to air pollution: a focus on ozone and nitrogen dioxide. J. Roy. Coll. Phys. Lond. 30 (1), 61–66.
Krupa, S.V., Legge, A.H., 1995. Air quality and its possible impacts on the terrestrial ecosystems of the North American Great Plains: an overview. Environ. Pollut. 88 (1), 1–11.
Li, M.M., Wang, T.J., Shu, L., Qu, Y.W., Xie, M., Liu, J.N., Wu, H., Kalsoom, U., 2021a. Rising surface ozone in China from 2013 to 2017: a response to the recent atmospheric warming or pollutant controls? Atmos. Environ. 246, 118130.
Li, K., Jacob, D.J., Liao, H., Qiu, Y.L., Shen, L., Zhai, S.X., Bates, K.H., Sulprizio, M.P., Song, S.J., Lu, X., Zhang, Q., Zheng, B., Zhang, Y.L., Zhang, J.Q., Lee, H.C., Kuk, S.K., 2021b. Ozone pollution in the North China Plain spreading into the late-winter haze season. Proc. Natl. Acad. Sci. U. S. A 118 (10), e2015797118.
Li, K., Jacob, D.J., Liao, H., Shen, L., Zhang, Q., Bates, K.H., 2019. Anthropogenic drivers of 2013-2017 trends in summer surface ozone in China. Proc. Natl. Acad. Sci. U. S. A 116 (2), 422–427.
Liu, H.Z., Liu, J.F., Liu, Y., Yi, K., Yang, H.Z., Xiang, S.L., Ma, J.M., Tao, S., 2021. Spatiotemporal variability and driving factors of ground-level summertime ozone pollution over eastern China. Atmos. Environ. 265, 118686.
Lu, X., Zhang, L., Chen, Y.F., Zhou, M., Zheng, B., Li, K., Liu, Y.M., Lin, J.T., Fu, T.M., Zhang, Q., 2019. Exploring 2016-2017 surface ozone pollution over China: source contributions and meteorological influences. Atmos. Chem. Phys. 19 (12), 8339–8361.

Malashock, D.A., DeLang, M.N., Becker, J.S., Serre, M.L., West, J.J., Chang, K.L., Cooper, O.R., Anenberg, S.C., 2022. Estimates of ozone concentrations and attributable mortality in urban, peri-urban and rural areas worldwide in 2019. Environ. Res. Lett. 17 (5), 054023.

Ma, Z.Q., Xu, J., Quan, W.J., Zhang, Z.Y., Lin, W.L., Xu, X.B., 2016. Significant increase of surface ozone at a rural site, north of eastern China. Atmos. Chem. Phys. 16 (6), 3969–3977.

Mao, J., Wang, L.L., Lu, C.H., Liu, J.D., Li, M.G., Tang, G.Q., Ji, D.S., Zhang, N., Wang, Y. S., 2020. Meteorological mechanism for a large-scale persistent severe ozone pollution event over eastern China in 2017. J. Environ. Sci. 92, 187–199.

Mousavinezhad, S., Choi, Y., Pouyaei, A., Ghahremanloo, M., Nelson, D.L., 2021. A comprehensive investigation of surface ozone pollution in China, 2015-2019: separating the contributions from meteorology and precursor emissions. Atmos. Res. 257, 105599.

Monks, P.S., Granier, C., Fuzzi, S., Stohl, A., Williams, M.L., Akimoto, H., Amann, M., Baklanov, A., Baltensperger, U., Bey, I., Blake, N., Blake, R.S., Carslaw, K., Cooper, O.R., Dentener, F., Fowler, D., Fragkou, E., Frost, G.J., Generoso, S., Ginoux, P., Grewe, V., Guenther, A., Hansson, H.C., Henne, S., Hjorth, J., Hofzumahaus, A., Huntrieser, H., Isaksen, I.S.A., Jenkin, M.E., Kaiser, J., Kanakidou, M., Klimont, Z., Kulmala, M., Laj, P., Lawrence, M.G., Lee, J.D., Liousse, C., Maione, M., McFiggans, G., Metzger, A., Mieville, A., Moussiopoulos, N., Orlando, J.J., O'Dowd, C.D., Palmer, P.I., Parrish, D.D., Petzold, A., Platt, U., Poschl, U., Prevot, A.S.H., Reeves, C.E., Reimann, S., Rudich, Y., Sellegri, K., Steinbrecher, R., Simpson, D., ten Brink, H., Theloke, J., van der Werf, G.R., Vautard, R., Vestreng, V., Vlachokostas, C., von Glasow, R., 2009. Atmospheric composition change - global and regional air quality. Atmos. Environ. 43 (33), 5268–5350.

Nagashima, T., Sudo, K., Akimoto, H., Kurokawa, J., Ohara, T., 2017. Long-term change in the source contribution to surface ozone over Japan. Atmos. Chem. Phys. 17 (13), 8231–8246.

Narumi, D., Kondo, A., Shimoda, Y., 2009. The effect of the increase in urban temperature on the concentration of photochemical oxidants. Atmos. Environ. 43 (14), 2348–2359.

Pedruzzi, R., Baek, B.H., Henderson, B.H., Aravanis, N., Pinto, J.A., Araujo, I.B., Nascimento, E.G.S., Reis, N.C., Moreira, D.M., Albuquerque, T.T.D., 2019. Performance evaluation of a photochemical model using different boundary conditions over the urban and industrialized metropolitan area of Vitoria, Brazil. Environ. Sci. Pollut. Control Ser. 26 (16), 16125–16144.

Qi, J.P., Mo, Z.W., Yuan, B., Huang, S., Huangfu, Y.B., Wang, Z.L., Li, X.B., Yang, S.X., Wang, W.J., Zhao, Y.M., Wang, X.M., Wang, W.W., Liu, K.X., Shao, M., 2021. An observation approach in evaluation of ozone production to precursor changes during the COVID-19 lockdown. Atmos. Environ. 262, 118618.

Ranmar, D.O., Matveev, V., Dayan, U., Peleg, M., Kaplan, J., Gertler, A.W., Luria, M., Kallos, G., Katsafados, P., Mahrer, Y., 2002. Impact of coastal transportation emissions on inland air pollution over Israel: utilizing numerical simulations, airborne measurements, and synoptic analyses. J. Geophys. Res. Atmos. 107 (D17), 4331.

Sahu, S.K., Liu, S.C., Liu, S., Ding, D., Xing, J., 2021. Ozone pollution in China: background and transboundary contributions to ozone concentration & related health effects across the country. Sci. Total Environ. 761, 144131.

Schultz, M.G., Schroder, S., Lyapina, O., Cooper, O.R., Galbally, I., Petropavlovskikh, I., von Schneidemesser, E., Tanimoto, H., Elshorbany, Y., Naja, M., Seguel, R.J., Dauert, U., Eckhardt, P., Feigenspan, S., Fiebig, M., Hjellbrekke, A.G., Hong, Y.D., Kjeld, P.C., Koide, H., Lear, G., Tarasick, D., Ueno, M., Wallasch, M., Baumgardner, D., Chuang, M.T., Gillett, R., Lee, M., Molloy, S., Moolla, R., Wang, T., Sharps, K., Adame, J.A., Ancellet, G., Apadula, F., Artaxo, P., Barlasina, M.E., Bogucka, M., Bonasoni, P., Chang, L., Colomb, A., Cuevas-Agullo, E., Cupeiro, M., Degorska, A., Ding, A.J., FrHlich, M., Frolova, M., Gadhavi, H., Gheusi, F., Gilge, S., Gonzalez, M.Y., Gros, V., Hamad, S.H., Helmig, D., Henriques, D., Hermansen, O., Holla, R., Hueber, J., Im, U., Jaffe, D.A., Komala, N., Kubistin, D., Lam, K.S., Laurila, T., Lee, H., Levy, I., Mazzoleni, C., Mazzoleni, L.R., McClure-Begley, A., Mohamad, M., Murovec, M., Navarro-Comas, M., Nicodim, F., Parrish, D., Read, K. A., Reid, N., Ries, N.R.L., Saxena, P., Schwab, J.J., Scorgie, Y., Senik, I., Simmonds, P., Sinha, V., Skorokhod, A.I., Spain, G., Spangl, W., Spoor, R., Springston, S.R., Steer, K., Steinbacher, M., Suharguniyawan, E., Torre, P., Trickl, T., Lin, W.L., Weller, R., Xu, X.B., Xue, L.K., Ma, Z.Q., 2017. Tropospheric Ozone Assessment Report: database and metrics data of global surface ozone observations. Elementa-Science of the Anthropocene 5 (4), 58.

Shu, L., Wang, T.J., Han, H., Xie, M., Chen, P.L., Li, M.M., Wu, H., 2020. Summertime ozone pollution in the Yangtze River Delta of eastern China during 2013-2017: synoptic impacts and source apportionment. Environ. Pollut. 257, 113631.

Sillman, S., 1995. The use of NO_y, H_2O_2, and HNO_3 as indicators for ozone-NO_x-hydrocarbon sensitivity in urban locations. J. Geophys. Res. Atmos. 100 (D7), 14175–14188.

Stauffer, R.M., Thompson, A.M., Martins, D.K., Clark, R.D., Goldberg, D.L., Loughner, C. P., Delgado, R., Dickerson, R.R., Stehr, J.W., Tzortziou, M.A., 2015. Bay breeze influence on surface ozone at Edgewood, MD during July 2011. J. Atmos. Chem. 72 (3–4), 335–353.

Sun, L.H., Cao, L., Ding, H.Y., Gao, M.M., Li, S.M., Chen, G., 2022. Influence of using different chemical mechanisms on simulations of ozone and its precursors in the troposphere of Shanghai, China. Atmos. Environ. 289, 119299.

Tang, H.Y., Liu, G., Zhu, J.G., Han, Y., Kobayashi, K., 2013. Seasonal variations in surface ozone as influenced by Asian summer monsoon and biomass burning in agricultural fields of the northern Yangtze River Delta. Atmos. Res. 122, 67–76.

Wang, T., Wu, Y.Y., Cheung, T.F., Lam, K.S., 2001. A study of surface ozone and the relation to complex wind flow in Hong Kong. Atmos. Environ. 35 (18), 3203–3215.

Wang, H., Lyu, X.P., Guo, H., Wang, Y., Zou, S.C., Ling, Z.H., Wang, X.M., Jiang, F., Zeren, Y.Z., Pan, W.Z., Huang, X.B., Shen, J., 2018a. Ozone pollution around a coastal region of South China Sea: interaction between marine and continental air. Atmos. Chem. Phys. 18 (6), 4277–4295.

Wang, Y., Guo, H., Lyu, X.P., Zhang, L.Y., Zeren, Y.Z., Zou, S.C., Ling, Z.H., 2019. Photochemical evolution of continental airmasses and their influence on ozone formation over the South China Sea. Sci. Total Environ. 673, 424–434.

Wang, Y., Guo, H., Zou, S.C., Lyu, X.P., Ling, Z.H., Cheng, H.R., Zeren, Y.Z., 2018b. Surface O-3 photochemistry over the South China Sea: application of a near-explicit chemical mechanism box model. Environ. Pollut. 234, 155–166.

Wang, Y., Liao, H., 2020. Effect of emission control measures on ozone concentrations in Hangzhou during G20 meeting in 2016. Chemosphere 261, 127729.

Wang, X.Q., Xiang, Y., Liu, W.T., Lv, L.H., Dong, Y.S., Fan, G.Q., Ou, J.P., Zhang, T.S., 2021. Vertical profiles and regional transport of ozone and aerosols in the Yangtze River Delta during the 2016 G20 summit based on multiple lidars. Atmos. Environ. 259, 118506.

Xie, Y., Wang, W., Wang, Q.L., 2018. Spatial distribution and temporal trend of tropospheric NO_2 over the wanjiang city belt of China. Adv. Meteorol. 2018, 6597186.

Xu, J.W., Huang, X., Wang, N., Li, Y.Y., Ding, A.J., 2021. Understanding ozone pollution in the Yangtze River Delta of eastern China from the perspective of diurnal cycles. Sci. Total Environ. 752, 141928.

Xu, X.B., Lin, W.L., Xu, W.Y., Jin, J.L., Wang, Y., Zhang, G., Zhang, X.C., Ma, Z.Q., Dong, Y.Z., Ma, Q.L., Yu, D.J., Li, Z., Wang, D.D., Zhao, H.R., 2020. Long-term changes of regional ozone in China: implications for human health and ecosystem impacts. Elementa-Science of the Anthropocene 8 (1), 13.

Yang, X.Y., Wu, K., Wang, H.L., Liu, Y.M., Gu, S., Lu, Y.Q., Zhang, X.L., Hu, Y.S., Ou, Y. H., Wang, S.G., Wang, Z.S., 2020. Summertime ozone pollution in Sichuan Basin, China: meteorological conditions, sources and process analysis. Atmos. Environ. 226, 117392.

Yi, F.J., McCarl, B.A., Zhou, X., Jiang, F., 2018. Damages of surface ozone: evidence from agricultural sector in China. Environ. Res. Lett. 13 (3), 034019.

Yin, Z.C., Cao, B.F., Wang, H.J., 2019. Dominant patterns of summer ozone pollution in eastern China and associated atmospheric circulations. Atmos. Chem. Phys. 19 (22), 13933–13943.

Zhang, H.L., Chen, G., Hu, J.L., Chen, S.H., Wiedinmyer, C., Kleeman, M., Ying, Q., 2014. Evaluation of a seven-year air quality simulation using the Weather Research and Forecasting (WRF)/Community Multiscale Air Quality (CMAQ) models in the eastern United States. Sci. Total Environ. 473, 275–285.

Zhang, S.J., Wu, Y., Zhao, B., Wu, X.M., Shu, J.W., Hao, J.M., 2017. City-specific vehicle emission control strategies to achieve stringent emission reduction targets in China's Yangtze River Delta region. J. Environ. Sci. 51, 75–87.

Zhao, S.P., Yu, Y., Yin, D.Y., Qin, D.H., He, J.J., Dong, L.X., 2018. Spatial patterns and temporal variations of six criteria air pollutants during 2015 to 2017 in the city clusters of Sichuan Basin, China. Sci. Total Environ. 624, 540–557.

Zhao, X.L., Zhou, W.Q., Han, L.J., Locke, D., 2019. Spatiotemporal variation in PM2.5 concentrations and their relationship with socioeconomic factors in China's major cities. Environ. Int. 133, 105145.

Zheng, J.Y., Zhong, L.J., Wang, T., Louie, P.K.K., Li, Z.C., 2010. Ground-level ozone in the Pearl River Delta region: analysis of data from a recently established regional air quality monitoring network. Atmos. Environ. 44 (6), 814–823.

Zhu, S.Q., Poetzscher, J., Shen, J.Y., Wang, S.Y., Wang, P., Zhang, H.L., 2021. Comprehensive insights into O_3 changes during he COVID-19 from O_3 formation regime and atmospheric oxidation capacity. Geophys. Res. Lett. 48 (10), e2021GL093668.